Electronic Supplementary Material (ESI) for RSC Advances.


SUPPLEMENTARY INFORMATION

# Full crystal structure, hydrogen bonding and spectroscopic, mechanical and thermodynamic properties of mineral uranopilite

*Francisco Colmenero,[a*] Jakub Plášil,[b] Vicente Timón,[a] Jiří Čejka[c]*

[a] Instituto de Estructura de la Materia (IEM), Consejo Superior de Investigaciones Científicas (CSIC), 28006 Madrid, Spain

[b] Institute of Physics ASCR, v.v.i., Na Slovance 2, 182 21, Praha 8, Czech Republic

[c]Mineralogicko-petrologické oddělení, Národní muzeum, Cirkusová 1740, 193 00 Praha 9, Czech Republic.

[*] E-mail: francisco.colmenero@iem.cfmac.csic.es

## Appendix A Methods

### A.1 Experimental

The diffuse reflectance infrared Fourier transform (DRIFT) spectrum of uranopilite was recorded from a natural crystal sample from Jáchymov (Czech Republic). The spectrum was collected using a Nicolet 6700 FTIR spectrometer coupled to an Olympus continuum microscope. The spectrum was collected in the wavenumber range from 4000 to 600 $cm^{-1}$ with a resolution of 5 $cm^{-1}$. All the manipulations of the infrared spectra were performed using the Omnic 9 software (Thermo Scientific).

Thermal analysis was conducted using the Setaram SetSys Evolution system (thermogravimetric and differential thermal analysis, TG-DTA) linked with a Thermo Scientific mass-spectrometer for the detection of the gases escaping during the thermal decomposition of the sample analyzed. The weight of the specimen was 7 mg. The sample was placed into a Pt crucible. The temperature range studied was 15–1190 °C and the velocity of increase in temperature was 10 °C/minute. A dynamical atmosphere with air-flow of 20 ml/minute was employed.

### A.2 First principles solid-state methods

#### A.2.1 Crystal structure

The crystal structure and properties of uranopilite were modeled with the Cambridge Serial Total Energy Program (CASTEP),[1] a component of the Materials Studio program suite.[2] The theoretical solid-state treatment employed in this work is based on Periodic Density Functional Theory using plane wave basis sets and pseudopotential functions to describe the internal atomic electrons.[3] The computations were carried out using the Perdew-Burke-Ernzerhof (PBE) energy-density functional[4] complemented with Grimme's empirical dispersion correction[5] (DFT-D2 approach). The specific pseudopotentials utilized were: (a) non-relativistic norm-conserving pseudopotentials[6] from CASTEP package for the S, O and H atoms; (b) a scalar relativistic norm-conserving pseudopotential for U atom generated from first principles recently.[7-8] This pseudopotential has been validated extensively for the investigation of the crystal structures, vibrational spectra and properties of uranyl containing materials.[7-18]

The unit cell of uranopilite is triclinic, space group $P\bar{1}$ (no. 2, Z = 2). The unit cell is extraordinarily complex and contains 158 atoms: 12 U, 2 S, 76 O and 68 H. Therefore, a very large number of valence electrons, 704, must be described explicitly in the calculations. The number of valence electrons per atom are 14, 6, 6 and 1 electrons for U, S, O and H, respectively, corresponding to the valence electron configurations: U[$6s^2 6p^6 6d^1 5f^3 7s^2$], S[$3s^2 3p^4$], $O[2s^2 2p^4]$, and $H[1s^1]$. The unit-cell parameters of uranopilite and the associated atomic positions were fully optimized by means of the Broyden–Fletcher–Goldfarb–Shanno (BFGS) technique.[19] A plane wave kinetic energy cut-off parameter of $\varepsilon$ = 1000 eV and a $k$-mesh[20] of 2 × 1 × 1 were utilized. These calculation parameters were chosen to attain a well converged crystal structure, energy and properties. The software REFLEX included in Materials Studio package of programs[2] was used to generate the X-ray powder diffraction patterns of uranopilite from the experimental and computed crystal structures.[21]

The impact of the inclusion of the Hubbard correction,[22] which allows for a correct description of the strong Coulomb repulsion between electrons in $f$ orbitals, was also evaluated. The introduction of this correction, improving drastically the description of materials containing uranium in which this element exists with IV oxidation state,[23-27] is shown to be unnecessary for uranopilite in Section 2.1 of the main

part of the paper. In fact, for a large number of materials in which uranium exists with VI oxidation state, the standard DFT description provides a reliable description of their structures and properties.[7-18,28-34]

### A.2.2 Elastic tensor and equation of state

The stiffness tensor[35] matrix elements required to calculate the mechanical properties of uranopilite and to study the mechanical stability of its crystal structure were determined using the finite deformation method (FDM).[36] The energy based techniques and density functional perturbation theory appear to be less efficient for this purpose than FDM.[36] It has been utilized successfully in previous works[8,12,13,15-18] for the computation of the elastic response of many solid uranyl-containing materials. The unit cell volumes in the vicinity of the equilibrium structure were computed by optimizing the uranopilite crystal structure under sixteen different external pressures with values in the range −1.0 to 9.0 GPa. The computed lattice volumes and associated pressures were then adjusted to a $4^{th}$ order Birch-Murnaghan equation of state[37] in order to extract the derivatives of the bulk modulus with respect to pressure. Angel's EOSFIT 5.2 code[38-39] was employed for fitting the pressure-volume data to the selected equation of state. The structural optimizations under pressure were also performed using the BFGS method. The 3D representations of the elastic properties of uranopilite as a function of the direction of the applied strain were obtained utilizing the ElAM software.[40]

### A.2.3 Infrared spectrum

The theoretical computation of the infrared spectrum of uranopilite was carried out by means of density functional perturbation theory.[41-42] The harmonic approximation of the interatomic force field was used for the calculation of the infrared vibrational frequencies and the corresponding band intensities. No scaling procedures were applied. These scaling procedures are frequently used to improve the computed infrared frequencies by correcting them empirically for the anharmonicity and remaining approximations used.[43] The unscaled vibrational spectra obtained using the DFPT method in previous works[7,9,12,13,16-18] have provided consistently accurate descriptions of the experimental spectra of uranyl-containing materials. Therefore, we considered advisable to employ the DFTP method without applying any kind of scaling procedure to determine the infrared spectrum of uranopilite.

### A.2.4 Thermodynamic properties

#### A.2.4.1 Fundamental thermodynamic properties.

Phonon calculations at the optimized crystal structure were performed to obtain the fundamental thermodynamic functions (ThF) of uranopilite. Density functional perturbation theory was employed to compute the phonon spectra at all the points of the Brillouin zone.[41] From the computed phonon spectra, the phonon dispersion curves and density of states were evaluated. The fundamental ThFs (Gibbs free energies, enthalpies, entropies, and specific heats) were obtained in terms of these functions using the quasi-harmonic approximation.[44] The thermodynamic functions of formation (ThFOF) and thermodynamic functions of reaction (ThFOR) were then evaluated in terms of the calculated fundamental ThFs using the methods described in the next subsections.[10-11,14]

#### A.2.4.2 Thermodynamic properties of formation.

The computed enthalpy and entropy functions, $(H_T - H_{298})^{calc}$ and $S_T^{calc}$, were employed to calculate the enthalpies of formation (EnOF) and Gibbs free energies of formation (GiFEOF) in terms of the elements using the expressions:[10,45]

$$\Delta_f H(T) = \Delta_f H^0 + \left(H_T - H_{298}\right)^{calc} + \sum_i^{elements} n_i (H_T - H_{298})_i^{exp} \qquad (A1)$$

$$\Delta_f G(T) = \Delta_f H(T) - T\left\{ S_T^{calc} - \sum_i^{elements} n_i (S_T)_i^{exp} \right\} \qquad (A2)$$

where $\Delta_f H^0$ is the enthalpy of formation at the standard state of the material being investigated (temperature of 295.15 K and pressure of 1 bar), and $(H_T - H_{298})_i^{exp}$ and $(S_T)_i^{exp}$ are the enthalpy and entropy functions of the elements forming part of this material with stoichiometric coefficients $n_i$, respectively. The $\Delta_f H^0$ value of used in this work is given in the main part of the paper. The thermodynamic functions for S, O and H were taken from JANAF (Joint Army-Navy-Air Force) thermochemical tables.[45] The functions for U were obtained from the Barin.[46] The reaction constants of the formation reactions were evaluated in terms of the corresponding GiFEOFs through the equation:[45]

$$\Delta G(T) = -\ R\ T\ Ln\ K \qquad (A3)$$

**A.2.4.3 Thermodynamic properties of reaction.**

The enthalpies of reaction (EnOR) and Gibbs free energies of reaction (GiFEOR) as a function of temperature were obtained from the calculated Gibbs free energy and entropy of formation functions, $\Delta_f G(T)^{calc}$ and $\Delta_f S(T)^{calc}$, by means of the equations:[11,45]

$$\Delta_r G(T) = \sum_i^{products} n_i \Delta_f G^i(T) - \sum_j^{reactants} n_j \Delta_f G^j(T) \qquad (A4)$$

$$\Delta_r H(T) = \Delta_r G(T) + T \cdot \Delta_r S(T) \qquad (A5)$$

where,

$$\Delta_r S(T) = \sum_i^{products} n_i \Delta_f S^i(T) - \sum_j^{reactants} n_j \Delta_f S^j(T) \qquad (A6)$$

In equations (A4) and (A6), $\Delta_f G^i(T)$ and $\Delta_f S^i(T)$ denote the Gibbs free energy and entropy of formation at temperature T of the compound $i$ entering in the reaction with stoichiometric coefficient $n_i$. The thermodynamic functions for $SO_3(g)$, $CO_2(g)$, $O_2(g)$, $H_2O(l)$, and $SiO_2(cr)$ were taken from JANAF thermochemical tables[45] and those of $H_2O_2(l)$ from Barin.[46] The reaction constants were obtained from the corresponding GiFEORs by using the equation (A3).

**Appendix B Detailed description of the experimental and computed infrared spectra. Infrared band assignment**

**B.1 The 2200-3750 $cm^{-1}$ region**

Fig. 4.D shows the experimental and theoretical infrared spectra of from 2700 to 3700 $cm^{-1}$. Going, as usual, from higher to lower wavenumbers, one first finds two small intensity bands, referred to as $A$ and $B$, located at 3689 and 3674 $cm^{-1}$, respectively. Due to their small intensity, these bands are not seen in Fig. 4.D and are displayed in Fig. 5.D which provides a detailed view of the experimental infrared spectrum from 3660 to 3750 $cm^{-1}$. These two bands do not appear in the theoretical spectrum and are identified as combination bands as detailed in Table S.4. As can be seen in Table S.3, the first of these bands was also encountered by Frost *et al*.[47] at 3695 $cm^{-1}$ in the infrared spectrum from the uranopilite sample from Midnite Mine (Washington, USA).

As can be observed in Fig. 4.D, the main part of the infrared spectrum of this region is very broad and may be resolved into eighteen different bands, ($a$) to ($r$). The vibrational frequencies of these bands are reproduced theoretically in a very satisfactory way (see Table S.4). All of these bands are assigned to $OH$ bond stretching vibrations.

Finally, the last two bands in this region, $s$ and $t$, situated at 2367 and 2344 $cm^{-1}$ (see Fig. 5.C) are not found in the computed spectrum and are recognized as combination bands. Band $t$ was also found by Frost *et al*.[47] in the experimental infrared spectrum of uranopilite sample from South Alligator River (Northern Territory, Australia) at 2348 $cm^{-1}$.

**B.2 The 1300-1750 $cm^{-1}$ region**

Fig. 4.B displays the experimental and theoretical infrared spectra from 1450 to 1750 $cm^{-1}$. region. Three main bands ($u$, $v$ and $x$), attributed to $HOH$ bending vibrations, are found at 1735, (1640, 1617) and (1540, 1524) $cm^{-1}$. These bands are well reproduced theoretically at 1705, (1632, 1627) and (1597, 1575) $cm^{-1}$. The bands $y$ and $z$, at 1438 and 1420 $cm^{-1}$ (Fig. 5.B), absent in the theoretical spectrum, are identified as a combination band and as an overtone, respectively (see Table S.4). The band $y$ was only found in the experimental infrared spectrum of Frost *et al*.[47] from the uranopilite sample from Apex Mine (Nevada, USA) at 1442 $cm^{-1}$. The overtone band $z$ was found by Frost *et al*.[47] in the experimental spectra of uranopilite from South River (Northern Territory, Australia), Ranger No. 1 deposit (Northern Territory, Australia) and Midnite Mine (Washington, USA) at 1421, 1421 and 1418 $cm^{-1}$, respectively

**B.3 The 1000-1200 $cm^{-1}$ region**

The experimental and computed infrared spectra of this spectral zone are compared in Fig. 4.B. The band $\alpha$, placed at 1162 $cm^{-1}$ is reproduced theoretically at 1178 $cm^{-1}$. It is ascribed to $UOH$ bending vibrations. The band $\beta$, at 1146 $cm^{-1}$, is found at 1098 $cm^{-1}$. Band $\gamma$ has two components at 1119 and 1103 $cm^{-1}$ which correspond to the calculated bands at 1075 and 1068 $cm^{-1}$. Bands $\beta$ and $\gamma$ are attributed to $UOH$ bending vibrations and water librations. Band $\delta$, at 1089 $cm^{-1}$, is linked to a pair of near theoretical bands located at 1051 and 1045 $cm^{-1}$. The first of these bands is assigned to $UOH$ bending vibrations and the second one to $UOH$ bending vibrations and water librations. Similarly, the band $\varepsilon$, at 1078 $cm^{-1}$, corresponds to two calculated bands at 1035 and 1023 $cm^{-1}$. Both bands are attributed to $UOH$ bending vibrations and water librations. Finally, the weak band $\zeta$, at 1010 $cm^{-1}$ (Fig. 5.A) is not

found in the theoretical spectrum and is recognized to be a combination band. It must be noted that Frost *et al.*[47] assigned all the bands in this region to sulfate asymmetric stretching vibrations, $\nu^a(SO^{2-}_4)$, except the band at 1010 $cm^{-1}$ which was assigned to sulfate symmetric stretching vibrations, $\nu^s(SO^{2-}_4)$. None of these assignments is supported by the present theoretical study. The vibrations localized at the sulfate units are not encountered in the vibrational atomic motions associated to the normal modes corresponding to these bands. For example, the sulfate symmetric stretching vibrations appear at the normal mode with wavenumber $\nu =$ 965 $cm^{-1}$ (see Fig. S.5) but the corresponding intensity is very small (4.6 $(D/\text{Å})^2/amu$). Although the band $\zeta$, found in the present work at 1010 $cm^{-1}$ is quite weak, it was detected by Frost *et al.*[47] in the experimental infrared spectra from three uranopilite samples from Ranger No. 1 deposit (Northern Territory, Australia), Apex Mine (Nevada, USA) and Midnite Mine (Washington, USA) at 1006, 1009 and 1010 $cm^{-1}$, respectively.

**2.4.4. The 600-1000 $cm^{-1}$ region**

The two theoretical bands placed at 998 and 988 $cm^{-1}$ correspond to the experimental band $\eta$ located at 978 $cm^{-1}$. Both bands are attributed to $UOH$ bending vibrations and water librations. The bands $\lambda$ and $\mu$ at 935 and 923 $cm^{-1}$ are calculated at 961 and 948 $cm^{-1}$, respectively and have the same assignment as band $\eta$. The band $\pi$ situated at 909 $cm^{-1}$ is linked to three very near theoretical bands situated at 892, 889 and 887 $cm^{-1}$. These three sub-bands are ascribed to a mixture of uranyl antisymmetric stretching vibrations, $\nu^a(UO^{2+}_2)$, $UOH$ bending vibrations and water librations. Band $\theta$, at 892 $cm^{-1}$, is reproduced in the theoretical spectrum at 878 $cm^{-1}$ and assigned to $UOH$ bending vibrations and water librations. The band $\sigma$, at 873 $cm^{-1}$ is ascribed, as band $\pi$, to a juxtaposition of uranyl antisymmetric stretching vibrations, $\nu^a(UO^{2+}_2)$, $UOH$ bending vibrations and water librations. While band $\eta$ was left without assignment by Frost *et al*.,[47] the bands $\lambda$, $\mu$, $\pi$, $\theta$ and $\sigma$ were assigned to uranyl antisymmetric stretching vibrations. Therefore, only bands $\pi$ and $\sigma$ were correctly assigned. However, even for these bands, the assignment is incomplete since the contribution of the $UOH$ bending vibrations and water librations is not included.

The bands $\tau$, $\xi$, $\chi$, $\rho$, $\phi$ and $\varphi$, placed at 823, 800, 775, 751, 708 and 675 $cm^{-1}$ are found in the theoretical spectrum at 842, 815, 785, 759, 709 and 690 $cm^{-1}$, respectively. The six bands are assigned to $UOH$ bending vibrations and water librations. Frost *et al*.[47] assigned band $\tau$ to uranyl symmetric stretching vibrations, $\nu^s(UO^{2+}_2)$. This assignment is not supported. In fact, uranyl symmetric stretching vibrations are not found in any of these normal modes. Finally, the band $\psi$, at 647 $cm^{-1}$ is very well reproduced theoretically at 645 $cm^{-1}$ and assigned to water librations only.

**2.4.5. The 400-600 $cm^{-1}$ region**

This spectral region was studied only theoretically. The bands in this region were included in the analysis because when the experimental spectrum was assigned it was found that they play a role in the interpretation of some infrared bands from the other regions (bands $A$, $B$ and $\zeta$). Four main bands, denoted as $\Pi$, $\Sigma$, $\Phi$, and $\Psi$, located at 552, 533, 475 and 406 $cm^{-1}$, respectively, were found in this region. Bands $\Pi$ and $\Phi$ are attributed to water librations only and bands $\Sigma$ and $\Psi$ are assigned to equatorial $UO$ bond stretching vibrations and water librations.

**Appendix C Thermal decomposition curve**

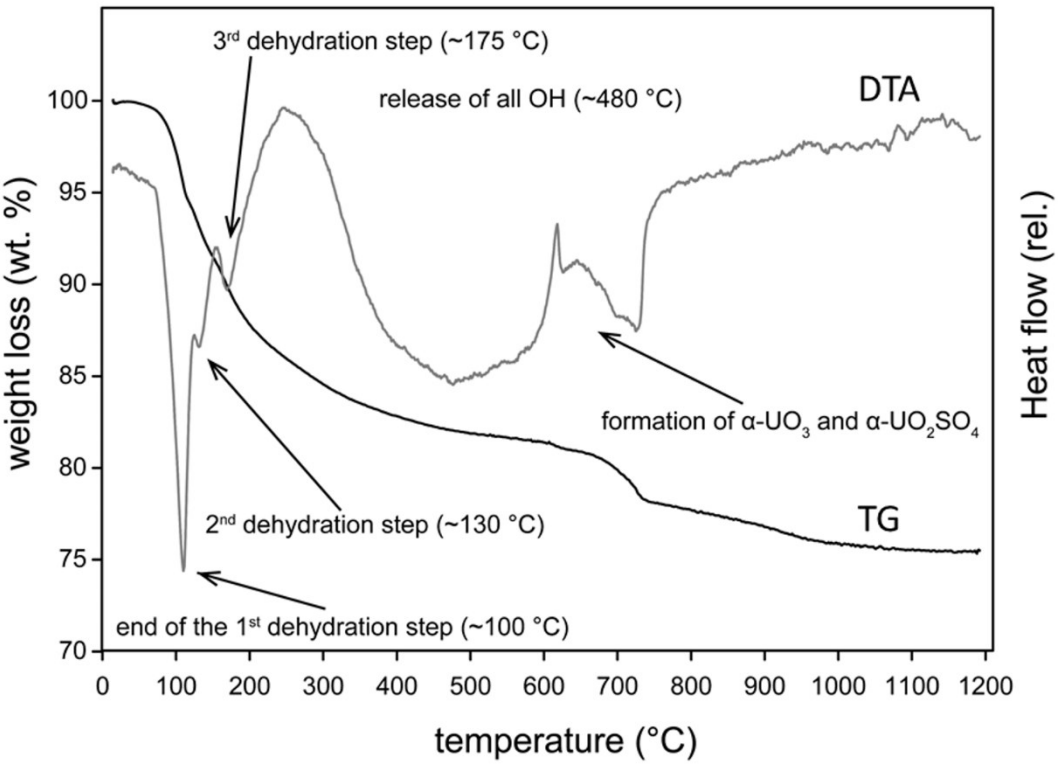


**Fig. S.1.** Thermal decomposition of uranopilite showing three-stage dehydration at elevated temperatures (first starting above 50 °C). The thermogravimetric (TG) curve and the differential thermal analysis (DTA) do not support the formation of a transition hydrated phase; only anhydrous phases are formed at elevated temperatures (above 600 °C).

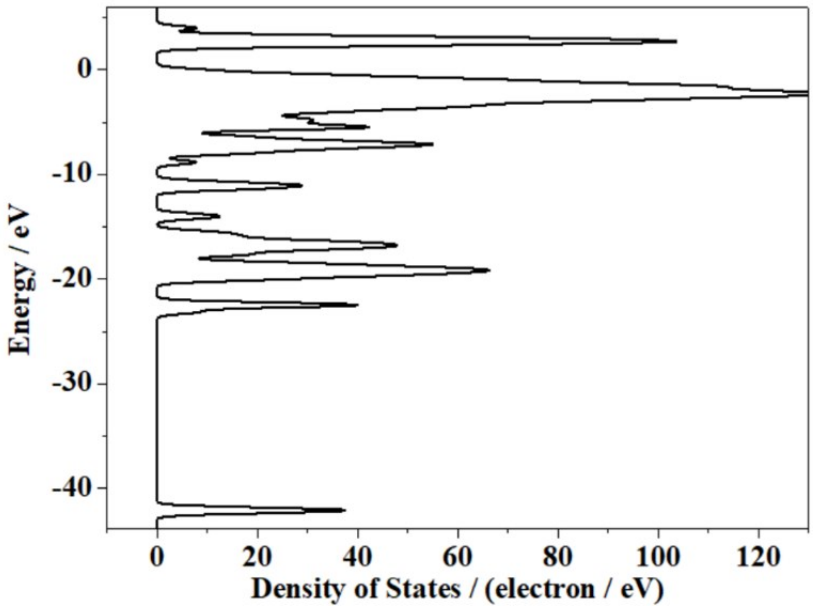


**Fig. S.2.** Computed density of states of uranopilite.

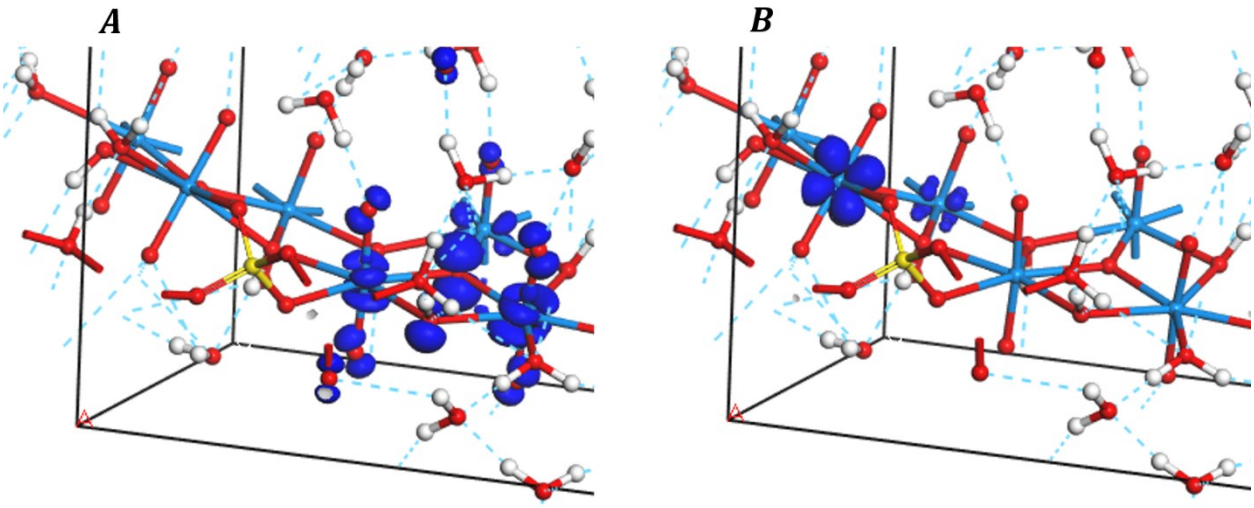


**Fig. S.3.** Frontier band functions in uranopilite: (A) Highest occupied band function; (B) Lowest unoccupied band function. Color code: U-Blue, S-Yellow, O-Red, H-White.

**Table S.1**. Bond lengths in uranopilite (in Å).

| Bond | Exp.[47] | Calc. | Bond | Exp.[47] | Calc. |
|---|---|---|---|---|---|
| **U-O** | | | | | |
| U1-O2 | 1.76(2) | 1.789 | U2-O4 | 1.81(2) | 1.785 |
| U1-O1 | 1.87(2) | 1.807 | U2-O3 | 1.83(2) | 1.807 |
| U1-O15 | 2.27(2) | 2.233 | U2-O16 | 2.27(2) | 2.249 |
| U1-OH22 | 2.39(2) | 2.460 | U2-OH19 | 2.39(2) | 2.381 |
| U1-O14 | 2.42(2 | 2.428 | U2-OH21 | 2.40(2) | 2.425 |
| U1-OH20 | 2.47(2) | 2.320 | U2-O18 | 2.42(2) | 2.400 |
| U1-OH19 | 2.52(2) | 2.557 | U2-OH22 | 2.49(2) | 2.495 |
| <U1-Oap> | 1.81(2) | 1.80 | <U2-Oap> | 1.82(2) | 1.80 |
| <U1-Oeq> | 2.41(2) | 2.40 | <U2-Oeq> | 2.39(2) | 2.39 |
| U3-O6 | 1.79(2) | 1.786 | U4-O7 | 1.79(2) | 1.788 |
| U3-O5 | 1.82(2) | 1.820 | U4-O8 | 1.80(2) | 1.791 |
| U3-O16 | 2.20(2) | 2.198 | U4-O15 | 2.18(2) | 2.213 |
| U3-OH23 | 2.42(2) | 2.362 | U4-OW26 | 2.39(2) | 2.568 |
| U3-O13 | 2.43(2) | 2.391 | U4-OH24 | 2.43(2) | 2.433 |
| U3-OW28 | 2.46(2) | 2.557 | U4-OH20 | 2.43(2) | 2.362 |
| U3-OH22 | 2.56(2) | 2.489 | U4-OW25 | 2.52(2) | 2.599 |
| <U3-Oap> | 1.80(2) | 1.80 | <U4-Oap> | 1.79(2) | 1.79 |
| <U3-Oeq> | 2.41(2) | 2.40 | <U4-Oeq> | 2.39(2) | 2.44 |
| U5-O9 | 1.72(2) | 1.786 | U6-O11 | 1.76(2) | 1.812 |
| U5-O10 | 1.81(2) | 1.806 | U6-O12 | 1.77(2) | 1.793 |
| U5-O15 | 2.22(2) | 2.166 | U6-O16 | 2.16(2) | 2.195 |
| U5-O17 | 2.37(2) | 2.422 | U6-OH23 | 2.42(2) | 2.414 |
| U5-OH24 | 2.38(2) | 2.419 | U6-OH21 | 2.44(2) | 2.432 |
| U5-OW29 | 2.48(2) | 2.556 | U6-OW27 | 2.48(2) | 2.396 |
| U5-OH19 | 2.51(2) | 2.495 | U6-OW30 | 2.54(2) | 2.537 |
| <U5-Oap> | 1.76(2) | 1.80 | <U6-Oap> | 1.76(2) | 1.80 |
| <U5-Oeq> | 2.39(2) | 2.41 | <U6-Oeq> | 2.41(2) | 2.39 |
| **S-O** | | | | | |
| S1-O18 | 1.45(2) | 1.487 | S1-O13 | 1.50(2) | 1.497 |
| S1-O14 | 1.49(2) | 1.486 | S1-O17 | 1.52(2) | 1.486 |

**Table S.2.** Most intense reflections in the X-ray powder pattern of uranopilite: (a) Difractogram computed from the experimental structure[47] (without the positions of the hydrogen atoms); (b) Difractogram calculated from the computed full crystal structure.

| **(a) Experimental[47]** | | | | **(b) Calculated** | | | $\Delta(2\theta)$ |
|---|---|---|---|---|---|---|---|
| $2\theta$ (°) | **d (Å)** | **I (%)** | **[hkl]** | $2\theta$ (°) | **d (Å)** | **I (%)** | |
| 12.60 | 7.02 | 100.00 | [002] | 12.65 | 6.99 | 100.00 | -0.05 |
| 9.65 | 9.16 | 46.25 | [011] | 9.51 | 9.29 | 36.44 | 0.13 |
| 12.91 | 6.85 | 33.03 | [101] | 12.98 | 6.81 | 28.95 | -0.08 |
| 20.92 | 4.24 | 24.92 | [013] | 20.80 | 4.27 | 24.19 | 0.12 |
| 30.59 | 2.92 | 21.32 | [-301] | 30.59 | 2.92 | 18.79 | 0.00 |
| 22.24 | 3.99 | 19.70 | [-202] | 22.18 | 4.00 | 17.74 | 0.05 |
| 11.07 | 7.99 | 16.25 | [-101] | 11.04 | 8.01 | 16.52 | 0.03 |
| 16.23 | 5.46 | 15.66 | [-121] | 15.79 | 5.61 | 11.63 | 0.45 |
| 24.66 | 3.61 | 14.84 | [-1-32] | 25.04 | 3.55 | 18.37 | -0.38 |
| 20.55 | 4.32 | 13.92 | [200] | 20.59 | 4.31 | 13.95 | -0.04 |
| 29.85 | 2.99 | 12.29 | [140] | 29.94 | 2.98 | 5.31 | -0.09 |
| 20.86 | 4.26 | 11.58 | [1-31] | 20.71 | 4.29 | 5.16 | 0.15 |
| 23.34 | 3.81 | 11.53 | [-1-31] | 23.59 | 3.77 | 5.41 | -0.26 |
| 22.68 | 3.92 | 10.90 | [1-13] | 22.91 | 3.88 | 7.61 | -0.23 |
| 27.46 | 3.25 | 10.06 | [-1-33] | 27.94 | 3.19 | 5.48 | -0.48 |
| 16.14 | 5.49 | 10.03 | [-112] | 15.84 | 5.59 | 10.09 | 0.30 |
| 30.79 | 2.90 | 9.86 | [-241] | 30.00 | 2.98 | 5.27 | 0.78 |
| 25.54 | 3.48 | 9.64 | [-230] | 25.06 | 3.55 | 5.94 | 0.48 |
| 26.50 | 3.36 | 9.26 | [2-31] | 26.24 | 3.39 | 12.43 | 0.27 |

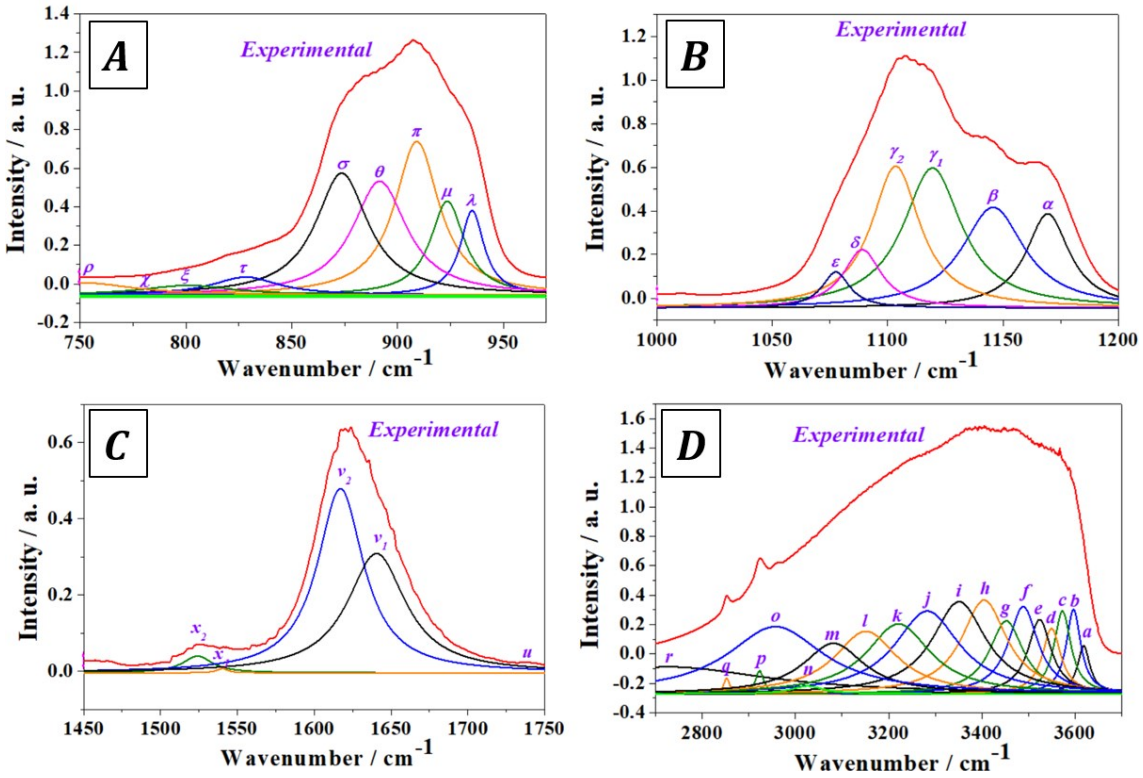


**Fig. S.4.** Resolution of some composite bands in the experimental infrared spectrum of uranopilite mineral into single band contributions: (A) Region 750-970 $cm^{-1}$; (B) Region 1000-1200 $cm^{-1}$; (C) Region 1450-1750 $cm^{-1}$; (B) Region 2700-3700 $cm^{-1}$.

**Fig. S.5.** The atomic motions associated to some infrared active vibrational normal modes of uranopilite. Color code: U-Blue, S-Yellow; O-Red, H-White.

- Mode $\nu =$ 3358 $cm^{-1}$ – $\nu(OH)$ – $OH$ bond stretching.

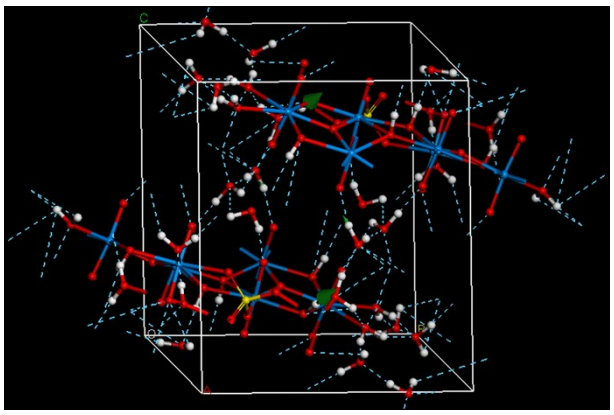

- Mode $\nu =$ 2898 $cm^{-1}$ – $\nu(OH)$ – $OH$ bond stretching.

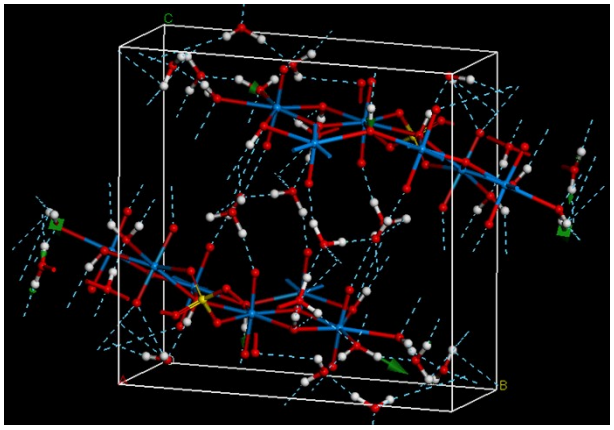

- Mode $\nu =$ 1632 $cm^{-1}$ – $\delta(HOH)$ – $HOH$ bending.

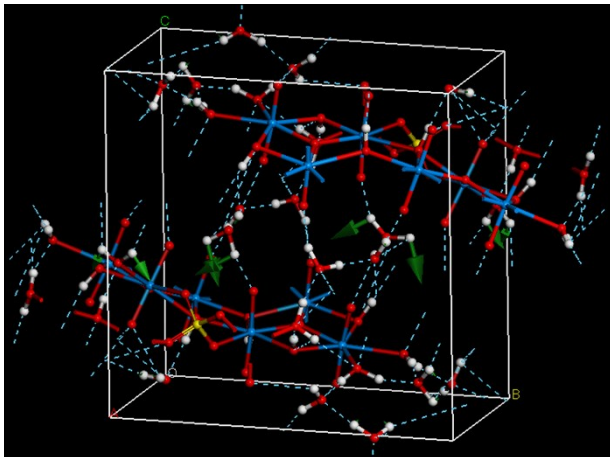

- Mode $\nu =$ 1178 $cm^{-1}$ – $\delta(UOH)$ – $UOH$ bending.

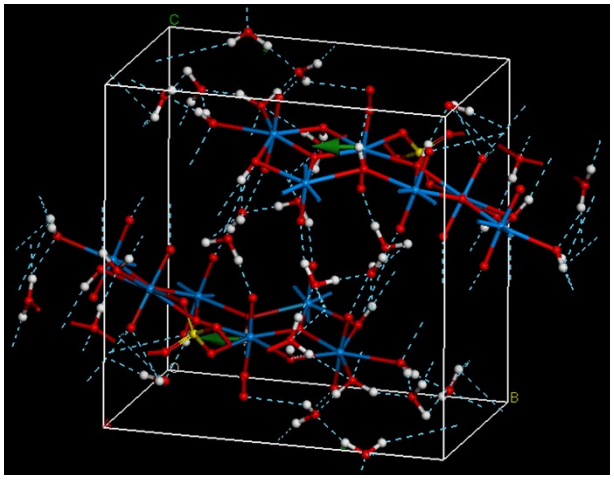

- Mode $\nu =$ 1068 $cm^{-1}$ – $\delta(UOH) + l(H_2O)$ – $UOH$ bending and water librations.

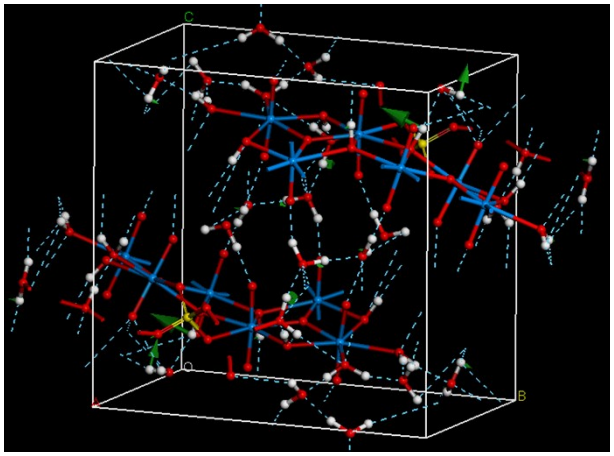

- Mode $\nu =$ 965 $cm^{-1}$ – $\nu^s\left(SO^{2-}_4\right) + \delta(UOH) + l(H_2O)$ – Symmetric sulfate stretching, $UOH$ bending and water librations.

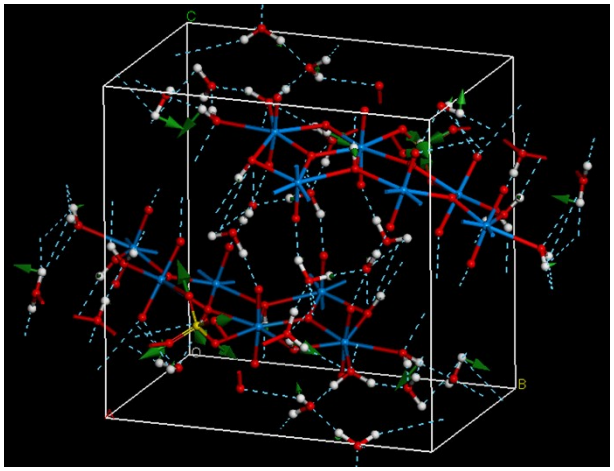

- Mode $\nu =$ 961 $cm^{-1}$ – $\delta(UOH) + l(H_2O)$ – $UOH$ bending and water librations.

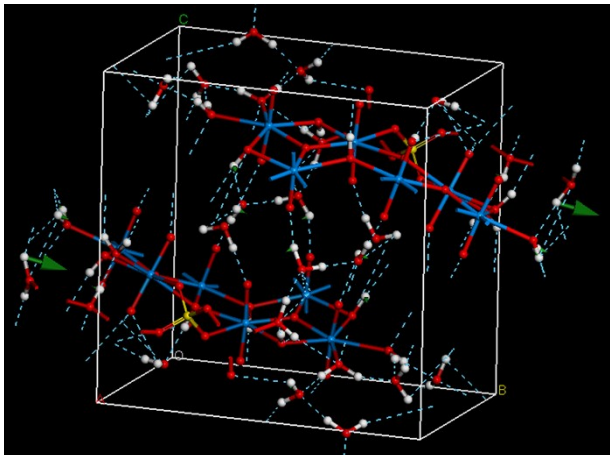

- Mode $\nu =$ 892 $cm^{-1}$ – $\nu^a\left(UO^{2+}_2\right) + \delta(UOH) + l(H_2O)$ – Antisymmetric uranyl stretching, $UOH$ bending and water librations.

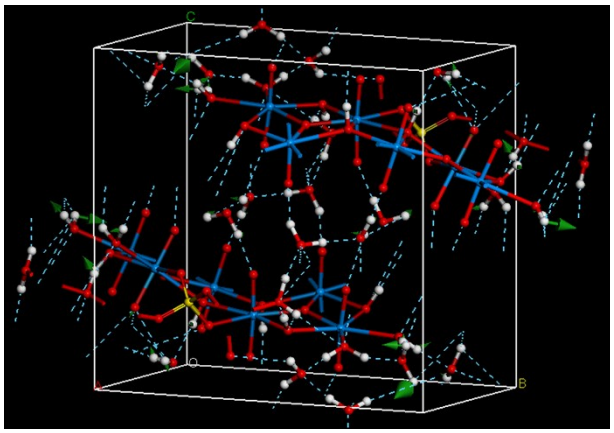

- Mode $\nu =$ 860 $cm^{-1}$ – $\nu^a\left(UO^{2+}_2\right) + \delta(UOH) + l(H_2O)$ – Antisymmetric uranyl stretching, $UOH$ bending and water librations.

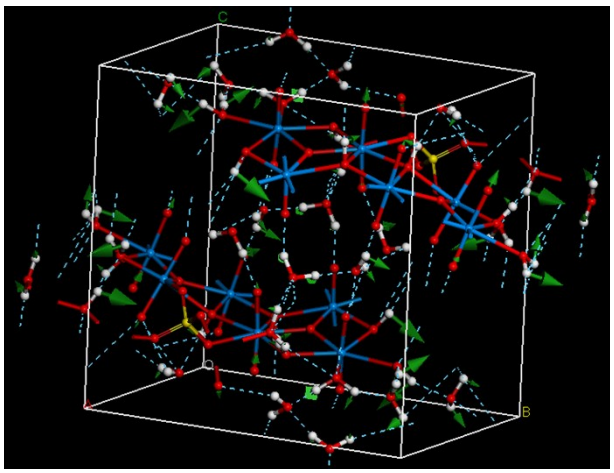

- Mode $\nu =$ 785 $cm^{-1}$ – $\delta(UOH) + l(H_2O)$ – $UOH$ bending and water librations.

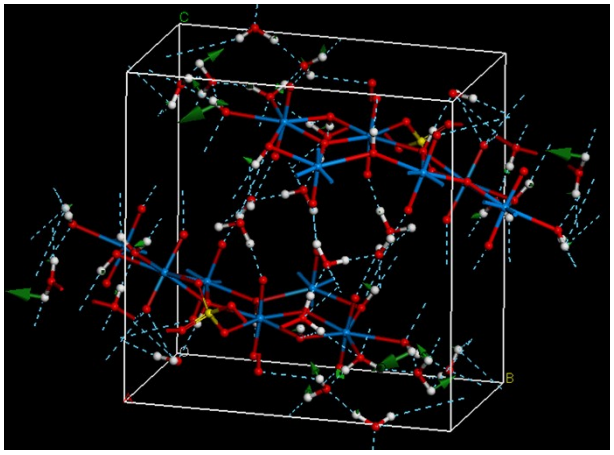

- Mode $\nu =$ 645 $cm^{-1}$ – $l(H_2O)$ – Water librations.

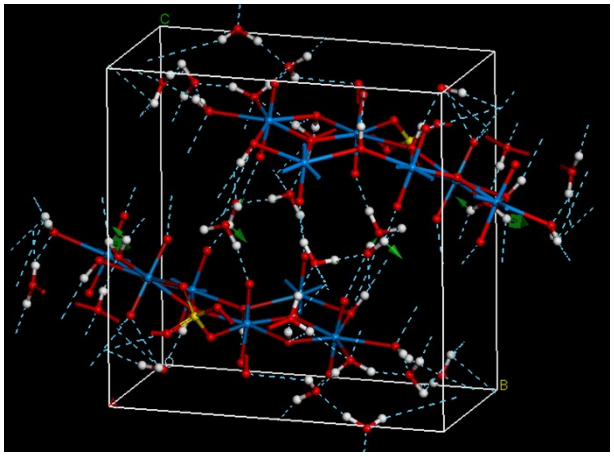

- Mode $\nu =$ 552 $cm^{-1}$ – $l(H_2O)$ – Water librations.

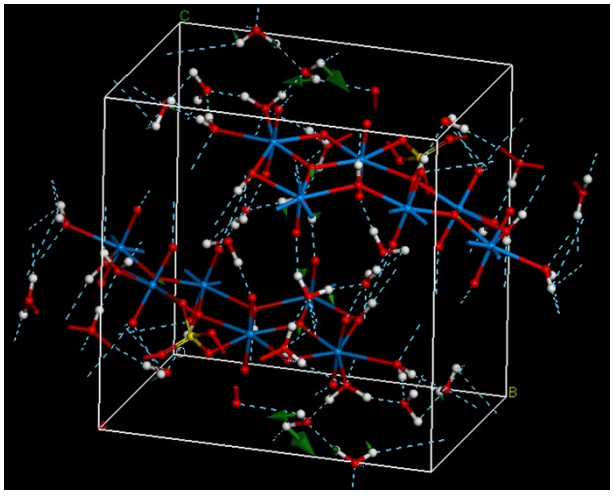

- Mode $\nu =$ 533 $cm^{-1}$ – $\nu(UO_{eq}) + l(H_2O)$ – Equatorial $UO_{eq}$ bond stretching vibrations and water librations.

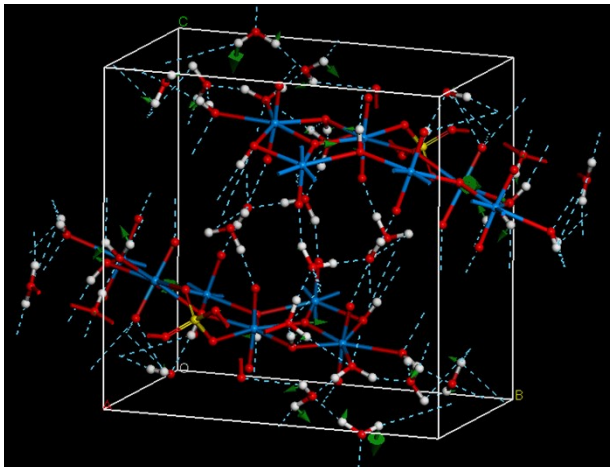

- Mode $\nu =$ 475 $cm^{-1}$ – $l(H_2O)$ – Water librations.

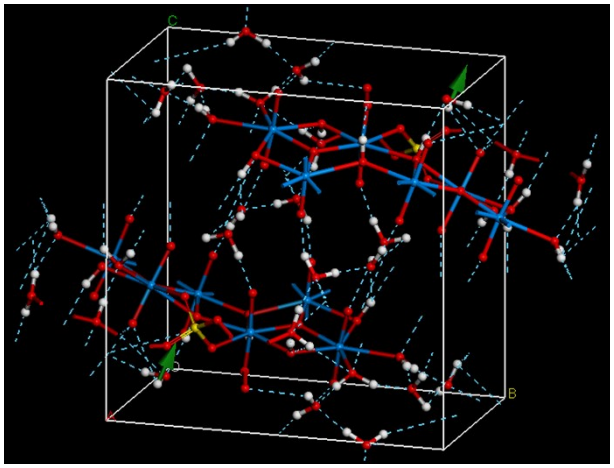

- Mode $\nu =$ 406 $cm^{-1}$ – $\nu(UO_{eq}) + l(H_2O)$ – Equatorial $UO_{eq}$ bond stretching vibrations and water librations.

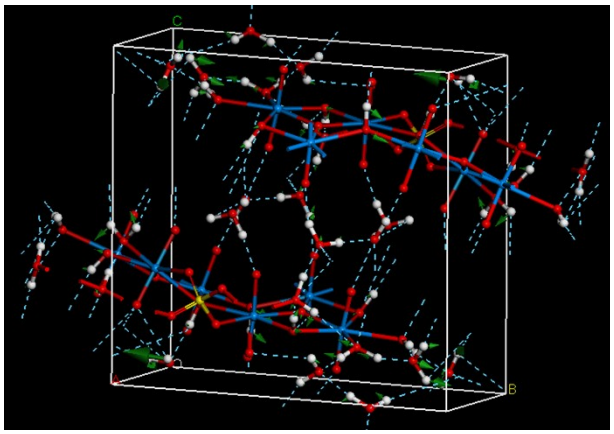

**Table S.3.** Comparison between the present experimental infrared band wavenumbers of uranopilite and those reported by Frost *et al*.[48]

| Band Name | Exp. Freq.($cm^{-1}$) [This work] | Exp. Freq.($cm^{-1}$) (South Alligator)[48] | Exp. Freq.($cm^{-1}$) (Ranger)[48] | Exp. Freq.($cm^{-1}$) (Apex)[48] | Exp. Freq.($cm^{-1}$) (Midnite)[48] |
|---|---|---|---|---|---|
| | | | $OH$ stretching region | | |
| $A$ | 3689 | - | - | - | 3695 |
| $B$ | 3674 | - | - | - | - |
| $a$ | 3619 | - | - | - | 3622 |
| $b$ | 3597 | - | - | 3600 | - |
| $c$ | 3573 | - | 3570 | - | 3588 |
| $d$ | 3550 | 3555 | - | 3561 | 3550 |
| $e$ | 3524 | - | - | 3517 | 3538 |
| $f$ | 3489 | 3471 | 3490 | 3510 | 3470 |
| $g$ | 3453 | - | - | 3428 | - |
| $h$ | 3405 | 3418 | 3397 | - | - |
| $i$ | 3351 | - | - | - | 3392 |
| $j$ | 3283 | 3268 | 3253 | 3274 | - |
| $k$ | 3221 | - | - | - | 3230 |
| $l$ | 3151 | 3136 | - | - | - |
| $m$ | 3082 | 3064 | 3074 | - | - |
| $n$ | 3026 | - | - | 3028 | 3049 |
| $o$ | 2957 | - | 2985 | - | - |
| $p$ | 2923 | - | - | - | - |
| $q$ | 2852 | 2877 | 2851 | - | - |
| $r$ | 2727 | - | - | 2698 | - |
| $s$ | 2367 | - | - | - | - |
| $t$ | 2344 | 2348 | - | - | - |
| | | | $HOH$ bending region | | |
| $u$ | 1735 | - | - | - | - |
| $v$ | 1640 | 1664 | - | - | - |
| | 1617 | 1625 | 1625 | 1623,1618 | 1627,1619 |
| $x$ | 1540 | 1575,1559,1540 | - | - | - |
| | 1524 | 1526,1511 | 1534 | 1535 | 1547 |
| $y$ | 1438 | - | - | 1442 | - |
| $z$ | 1420 | 1421 | 1421 | - | 1418 |
| | | | 1000-1200 $cm^{-1}$ region | | |
| $\alpha$ | 1162 | - | 1159 | 1170 | |
| $\beta$ | 1146 | 1138 | 1141 | 1138 | 1141 |
| $\gamma$ | 1119 | 1118 | 1118 | 1113 | 1116 |
| | 1103 | 1100 | 1099 | 1097 | 1102 |
| $\delta$ | 1089 | - | - | - | 1096 |
| $\varepsilon$ | 1078 | 1072 | 1072 | 1070 | - |
| - | - | 1031 | - | 1037 | 1032 |
| $\zeta$ | 1010 | - | 1006 | 1009 | 1010 |
| | | | 600-1000 $cm^{-1}$ region | | |
| $\eta$ | 978 | 982 | - | - | 999 |
| $\lambda$ | 935 | 932 | 941 | - | 941 |
| $\mu$ | 923 | - | 929 | 925 | 929 |
| $\pi$ | 909 | 912 | 910 | 911 | 901 |
| $\theta$ | 892 | 888 | 884 | 892 | - |
| $\sigma$ | 873 | 863 | - | - | 866 |
| $\tau$ | 823 | 838 | 838 | 830,821 | 841,828 |
| $\xi$ | 800 | - | 807 | - | - |
| $\chi$ | 775 | 788 | - | 798 | 792 |
| $\rho$ | 751 | 740 | - | 746 | 759,747 |
| $\phi$ | 708 | 703 | - | - | - |
| $\varphi$ | 675 | - | - | 674 | 687 |
| $\psi$ | 647 | - | - | - | 662,652 |

**Table S.4.** Vibrational frequencies of the bands from the observed and calculated infrared spectra of uranopilite. The calculated band intensities and assignments are also given.

| Band Name | Exp. Freq. ($cm^{-1}$) | Calc. Freq. ($cm^{-1}$) | Int. [$(D/Å)^2/amu$] | Assignment |
|---|---|---|---|---|
| | | | **2200-3750 $cm^{-1}$ region** | |
| $A$ | 3689 | - | - | $2{\cdot}\nu_1+\nu_2$=2·1640+406=3686 [$2{\cdot}\upsilon_1+\Psi$] |
| $B$ | 3674 | - | - | $\nu_1+\nu_2+\nu_3$=1640+1617+406=3663 [$\upsilon_1+\upsilon_2+\Psi$] |
| $a$ | 3619 | 3628 | 6.02 | $\nu(OH)$ |
| $b$ | 3597 | 3601 | 8.77 | " |
| $c$ | 3573 | 3589 | 10.39 | " |
| $d$ | 3550 | 3562 | 14.09 | " |
| $e$ | 3524 | 3510 | 22.63 | " |
| $f$ | 3489 | 3489 | 11.57 | " |
| $g$ | 3453 | 3433 | 63.34 | " |
| $h$ | 3405 | 3410 | 50.34 | " |
| $i$ | 3351 | 3358 | 94.74 | " |
| | | 3345 | 72.82 | " |
| $j$ | 3283 | 3304 | 18.54 | " |
| $k$ | 3221 | 3208 | 34.22 | " |
| $l$ | 3151 | 3141 | 74.15 | " |
| $m$ | 3082 | 3109 | 203.24 | " |
| | | 3091 | 251.64 | " |
| $n$ | 3026 | 3053 | 162.85 | " |
| $o$ | 2957 | 3003 | 193.31 | " |
| $p$ | 2923 | 2898 | 364.62 | " |
| $q$ | 2852 | 2859 | 169.66 | " |
| $r$ | 2727 | 2760 | 129.57 | " |
| $s$ | 2367 | - | - | $\nu_1+\nu_2$=1617+751=2368 [$\upsilon_2+\rho$] |
| $t$ | 2344 | - | - | $\nu_1+\nu_2$=1640+708=2348 [$\upsilon_1+\phi$] |
| | | | 1300-1750 $cm^{-1}$ region | |
| $u$ | 1735 | 1705 | 2.59 | $\delta(HOH)$ |
| $v$ | 1640 | 1632 | 20.70 | " |
| | 1617 | 1627 | 18.84 | " |
| $x$ | 1540 | 1597 | 8.78 | " |
| | 1524 | 1575 | 5.37 | " |
| $y$ | 1438 | - | - | $\nu_1+\nu_2$=751+675=1426 [$\rho+\varphi$] |
| $z$ | 1420 | - | - | $2{\cdot}\nu_1$=2·708=1416 [$2{\cdot}\phi$] |
| | | | 1000-1200 $cm^{-1}$ region | |
| $\alpha$ | 1162 | 1178 | 7.79 | $\delta(UOH)$ |
| $\beta$ | 1146 | 1098 | 36.48 | $\delta(UOH)+l(H_2O)$ |
| $\gamma$ | 1119 | 1075 | 45.38 | " |
| | 1103 | 1068 | 47.32 | " |
| $\delta$ | 1089 | 1051 | 20.27 | $\delta(UOH)$ |
| | | 1045 | 24.10 | $\delta(UOH)+l(H_2O)$ |
| $\varepsilon$ | 1078 | 1035 | 11.49 | " |
| | | 1023 | 15.12 | " |
| $\zeta$ | 1010 | - | - | $\nu_1+\nu_2$=533+475=1008 [$\Sigma+\Phi$] |
| | | | 600-1000 $cm^{-1}$ region | |
| $\eta$ | 978 | 998 | 18.35 | $\delta(UOH)+l(H_2O)$ |
| | | 988 | 17.12 | " |
| $\lambda$ | 935 | 961 | 11.61 | " |
| $\mu$ | 923 | 948 | 9.54 | " |
| $\pi$ | 909 | 892 | 43.47 | $\nu^a(UO_2^{2+})+\delta(UOH)+l(H_2O)$ |
| | | 889 | 29.15 | " |
| | | 887 | 25.05 | " |
| $\theta$ | 892 | 878 | 25.93 | $\delta(UOH)+l(H_2O)$ |
| $\sigma$ | 873 | 860 | 32.16 | $\nu^a(UO_2^{2+})+\delta(UOH)+l(H_2O)$ |
| $\tau$ | 823 | 842 | 58.85 | $\delta(UOH)+l(H_2O)$ |
| $\xi$ | 800 | 815 | 28.23 | " |
| $\chi$ | 775 | 785 | 12.04 | " |
| $\rho$ | 751 | 759 | 8.56 | " |
| $\phi$ | 708 | 709 | 4.91 | " |
| $\varphi$ | 675 | 690 | 5.75 | " |
| $\psi$ | 647 | 645 | 14.63 | $l(H_2O)$ |
| | | | 400-600 $cm^{-1}$ region | |
| $\Pi$ | - | 552 | 29.26 | $l(H_2O)$ |
| $\Sigma$ | - | 533 | 33.13 | $\nu(UO_{eq})+l(H_2O)$ |

| | | | | |
|---|---|---|---|---|
| Φ | - | 475 | 17.61 | $l(H_2O)$ |
| Ψ | - | 406 | 10.51 | $\nu(UO_{eq}) + l(H_2O)$ |

**Table S.5.** Computed elastic constants of uranopilite. The Voigt convention is employed for the indices of the matrix elements of the elasticity tensor (a pair of cartesian indices are contracted into a single integer: $1 \leq i \leq 6$: $xx \rightarrow 1, yy \rightarrow 2, zz \rightarrow 3, yz \rightarrow 4, xz \rightarrow 5, xy \rightarrow 6$). All the values are given in GPa.

| $ij$ | $C_{ij}$ |
|---|---|
| 11 | 50.35 |
| 22 | 41.51 |
| 33 | 22.94 |
| 44 | 8.28 |
| 55 | 6.15 |
| 66 | 15.12 |
| 12 | 14.32 |
| 13 | 11.49 |
| 14 | -2.26 |
| 15 | -4.53 |
| 16 | 0.53 |
| 23 | 13.60 |
| 24 | -6.06 |
| 25 | -1.45 |
| 26 | -0.19 |
| 34 | 0.02 |
| 35 | 5.74 |
| 36 | -2.14 |
| 45 | 0.02 |
| 46 | -0.61 |
| 56 | 2.02 |

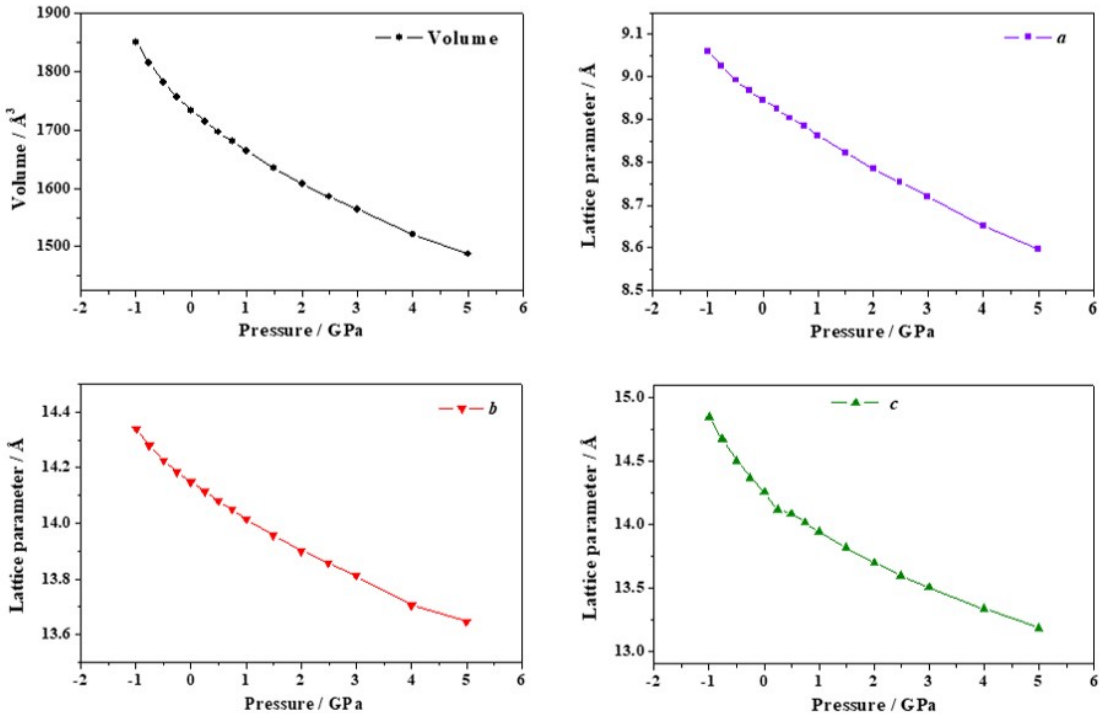


**Fig. S.6.** Calculated unit cell volume and lattice parameters of uranopilite as a function of the applied isotropic external pressure.

**Table S.6.** Calculated compressibility ($k_V = -1/V \cdot (\partial V/\partial P)_P$) of uranopilite under isotropic pressures from -0.5 to 4.0 GPa.

| **P (GPa)** | $k_V(TPa^{-1})$ |
|---|---|
| -0.50 | 63.44 |
| 0.00 | 47.69 |
| 0.50 | 40.70 |
| 1.00 | 36.94 |
| 1.50 | 33.68 |
| 2.00 | 30.35 |
| 2.50 | 27.70 |
| 3.00 | 26.77 |
| 3.50 | 27.76 |
| 4.00 | 28.83 |

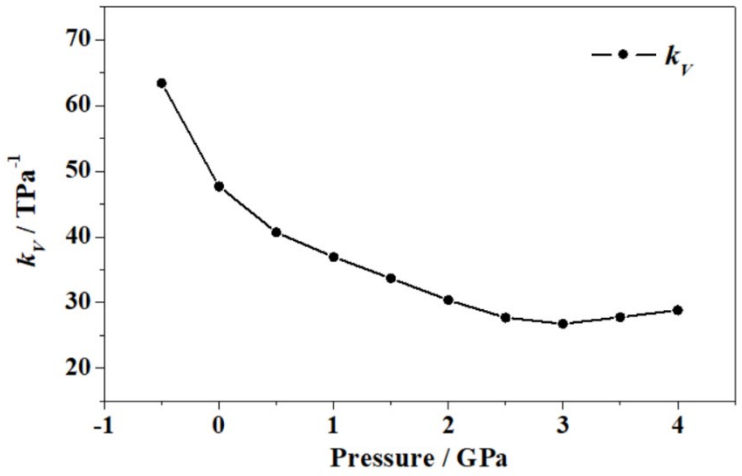


**Fig. S.7.** Calculated compressibility ($k_V = -1/V \cdot (\partial V/\partial P)_P$) of uranopilite under isotropic pressures from -0.5 to 4.0 GPa.

**Table S.7.** Calculated unit cell volumes and lattice parameters of uranopilite as a function of the external pressure applied along the direction of minimum compressibility.

| P (GPa) | Vol. (Å$^3$) | *a* (Å) | *b* (Å) | *c* (Å) | $\alpha\,(deg)$ | $\beta\,(deg)$ | $\gamma(deg)$ |
|---|---|---|---|---|---|---|---|
| -0.0593 | 1738.6614 | 8.9821 | 14.0792 | 14.3089 | 94.68 | 99.12 | 101.51 |
| -0.0324 | 1735.7281 | 8.9613 | 14.1163 | 14.2848 | 94.59 | 99.19 | 101.59 |
| -0.0191 | 1734.4859 | 8.9527 | 14.1325 | 14.2742 | 94.56 | 99.21 | 101.62 |
| -0.0068 | 1734.1442 | 8.9500 | 14.1369 | 14.2715 | 94.54 | 99.22 | 101.63 |
| 0.0029 | 1733.4378 | 8.9460 | 14.1417 | 14.2678 | 94.55 | 99.22 | 101.64 |
| 0.0073 | 1732.7031 | 8.9423 | 14.1468 | 14.2629 | 94.55 | 99.22 | 101.64 |
| 0.0131 | 1733.3383 | 8.9393 | 14.1513 | 14.2690 | 94.52 | 99.23 | 101.66 |
| 0.0208 | 1732.8179 | 8.9365 | 14.1556 | 14.2650 | 94.53 | 99.23 | 101.66 |
| 0.0239 | 1732.1363 | 8.9336 | 14.1605 | 14.2596 | 94.53 | 99.24 | 101.66 |
| 0.0267 | 1731.6503 | 8.9324 | 14.1606 | 14.2586 | 94.53 | 99.25 | 101.67 |
| 0.0329 | 1731.1806 | 8.9308 | 14.1549 | 14.2645 | 94.55 | 99.25 | 101.69 |
| 0.0473 | 1730.8036 | 8.9304 | 14.1623 | 14.2524 | 94.53 | 99.24 | 101.67 |
| 0.0613 | 1728.7138 | 8.9127 | 14.1900 | 14.2376 | 94.48 | 99.27 | 101.70 |

**Table S.8.** Calculated compressibilities ($k_V = -1/V \cdot (\partial V/\partial P)_P$) of uranopilite for external pressures applied along the direction of minimum compressibility between 0.005 and 0.025 GPa.

| **P (GPa)** | $k_V(TPa^{-1})$ | **P (GPa)** | $k_V(TPa^{-1})$ | **P (GPa)** | $k_V(TPa^{-1})$ |
|---|---|---|---|---|---|
| 0.005 | 95.25 | 0.013 | -56.32 | 0.021 | 123.20 |
| 0.007 | -5.93 | 0.015 | -11.01 | 0.023 | 128.31 |
| 0.009 | -63.57 | 0.017 | 43.42 | 0.025 | 106.74 |
| 0.011 | -77.90 | 0.019 | 92.30 | - | - |

**Table S.9.** Calculated unit cell volumes and lattice parameters of uranopilite as a function of the external pressure applied along the direction of minimum Poisson's ratio.

| P (GPa) | Vol. (Å$^3$) | *a* (Å) | *b* (Å) | *c* (Å) | $\alpha\,(deg)$ | $\beta\,(deg)$ | $\gamma(deg)$ |
|---|---|---|---|---|---|---|---|
| -0.0853 | 1735.1615 | 8.9586 | 14.1928 | 14.2011 | 94.44 | 99.08 | 101.64 |
| -0.0415 | 1734.3024 | 8.9514 | 14.1614 | 14.2422 | 94.50 | 99.16 | 101.63 |
| -0.0309 | 1733.6391 | 8.9487 | 14.1507 | 14.2542 | 94.53 | 99.19 | 101.63 |
| 0.0029 | 1733.4378 | 8.9460 | 14.1417 | 14.2678 | 94.55 | 99.22 | 101.64 |
| 0.0087 | 1732.8137 | 8.9448 | 14.1333 | 14.2738 | 94.58 | 99.23 | 101.62 |
| 0.0122 | 1732.6281 | 8.9449 | 14.1342 | 14.2708 | 94.58 | 99.22 | 101.63 |
| 0.0196 | 1732.7835 | 8.9439 | 14.1322 | 14.2769 | 94.57 | 99.24 | 101.64 |
| 0.0251 | 1732.9622 | 8.9427 | 14.1321 | 14.2807 | 94.56 | 99.25 | 101.64 |
| 0.0298 | 1732.4874 | 8.9416 | 14.1196 | 14.2907 | 94.61 | 99.25 | 101.61 |
| 0.0327 | 1732.1062 | 8.9406 | 14.1153 | 14.2941 | 94.62 | 99.26 | 101.60 |
| 0.0422 | 1731.8172 | 8.9398 | 14.1105 | 14.2983 | 94.65 | 99.26 | 101.59 |
| 0.0983 | 1730.6244 | 8.9298 | 14.0597 | 14.3653 | 94.78 | 99.40 | 101.57 |

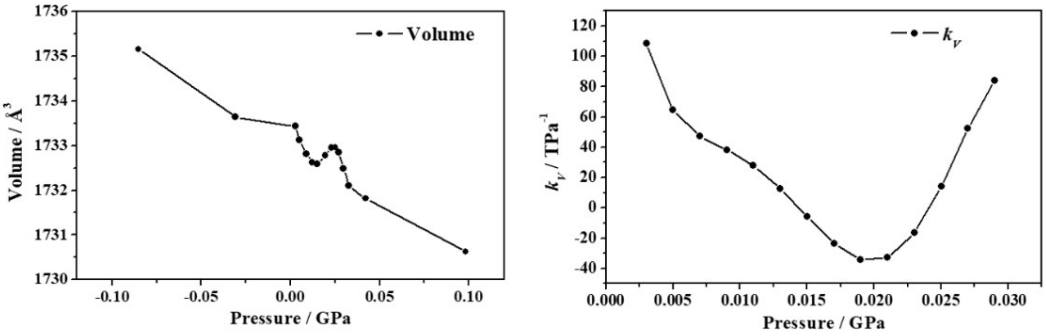


**Fig. S.8**. Unit cell volumes and compressibilities ($k_V$) of uranopilite calculated as a function of the external pressure applied along the minimum Poisson's ratio direction

**Table S.10.** Calculated compressibilities ($k_V = -1/V \cdot (\partial V/\partial P)_P$) of uranopilite for external pressures applied along the direction of minimum Poisson's ratio between 0.003 and 0.009 GPa.

| **P (GPa)** | $k_V(TPa^{-1})$ | **P (GPa)** | $k_V(TPa^{-1})$ | **P (GPa)** | $k_V(TPa^{-1})$ |
|---|---|---|---|---|---|
| 0.003 | 108.84 | 0.013 | 12.79 | 0.023 | -16.43 |
| 0.005 | 64.51 | 0.015 | -5.81 | 0.025 | 14.24 |
| 0.007 | 47.09 | 0.017 | -23.38 | 0.027 | 52.45 |
| 0.009 | 38.23 | 0.019 | -34.17 | 0.029 | 84.02 |
| 0.011 | 27.94 | 0.021 | -32.87 | - | - |

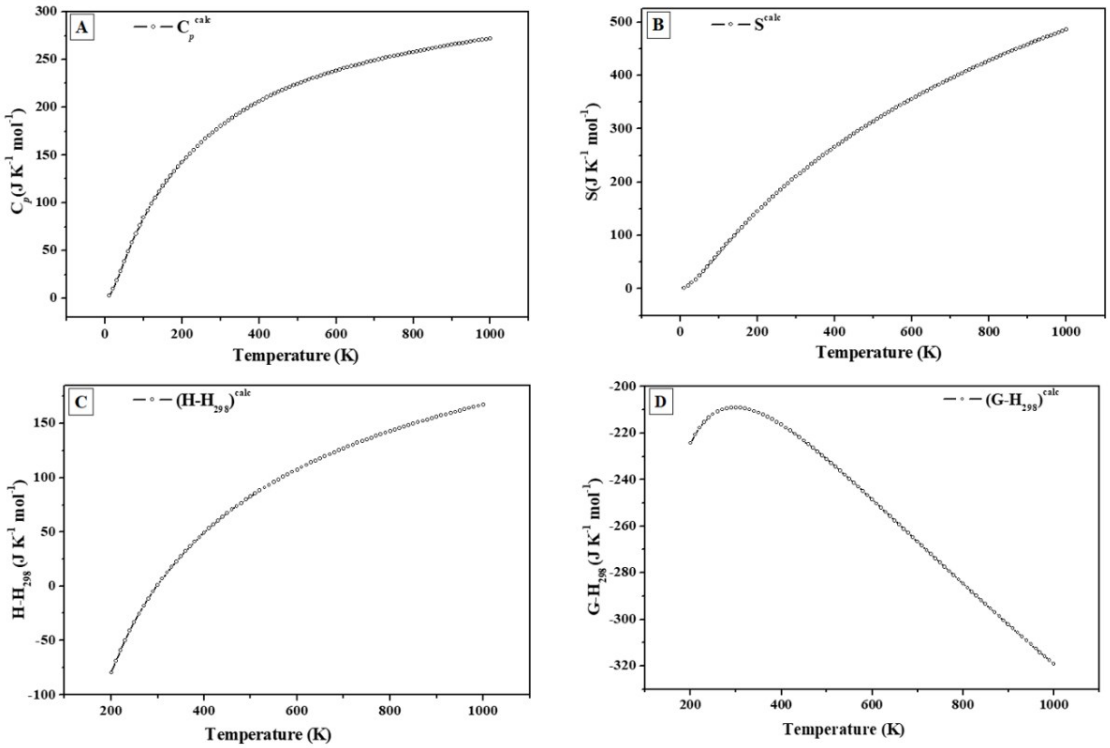


**Fig. S.9.** Computed fundamental thermodynamic functions of uranopilite: (A) Heat capacity; (B) Entropy; (C) Enthalpy; (D) Free energy.

**Table S.11.** Calculated isobaric heat capacity function, $C_P$, of uranopilite. Temperature and heat capacity values are given in K and J·K$^{-1}$·mol$^{-1}$ units, respectively.

| T | $C_P$ | T | $C_P$ | T | $C_P$ |
|---|---|---|---|---|---|
| 10 | 2.73791 | 350 | 194.30785 | 690 | 247.97954 |
| 20 | 9.79348 | 360 | 196.84737 | 700 | 248.95673 |
| 30 | 18.59893 | 370 | 199.29728 | 710 | 249.91556 |
| 40 | 28.37687 | 380 | 201.66132 | 720 | 250.85677 |
| 50 | 38.53585 | 390 | 203.94312 | 730 | 251.78101 |
| 60 | 48.64947 | 400 | 206.14622 | 740 | 252.68891 |
| 70 | 58.42798 | 410 | 208.27408 | 750 | 253.58107 |
| 80 | 67.69908 | 420 | 210.33004 | 760 | 254.45803 |
| 90 | 76.38579 | 430 | 212.31736 | 770 | 255.32033 |
| 100 | 84.47787 | 440 | 214.23918 | 780 | 256.16843 |
| 110 | 92.00532 | 450 | 216.09853 | 790 | 257.00281 |
| 120 | 99.01844 | 460 | 217.89833 | 800 | 257.82389 |
| 130 | 105.57461 | 470 | 219.64138 | 810 | 258.63208 |
| 140 | 111.73036 | 480 | 221.33040 | 820 | 259.42776 |
| 150 | 117.53707 | 490 | 222.96796 | 830 | 260.21128 |
| 160 | 123.03913 | 500 | 224.55654 | 840 | 260.98299 |
| 170 | 128.27357 | 510 | 226.09849 | 850 | 261.74319 |
| 180 | 133.27051 | 520 | 227.59608 | 860 | 262.49220 |
| 190 | 138.05410 | 530 | 229.05146 | 870 | 263.23030 |
| 200 | 142.64344 | 540 | 230.46665 | 880 | 263.95774 |
| 210 | 147.05367 | 550 | 231.84362 | 890 | 264.67479 |
| 220 | 151.29685 | 560 | 233.18421 | 900 | 265.38168 |
| 230 | 155.38267 | 570 | 234.49015 | 910 | 266.07864 |
| 240 | 159.31912 | 580 | 235.76310 | 920 | 266.76589 |
| 250 | 163.11296 | 590 | 237.00464 | 930 | 267.44364 |
| 260 | 166.77006 | 600 | 238.21624 | 940 | 268.11206 |
| 270 | 170.29569 | 610 | 239.39930 | 950 | 268.77136 |
| 280 | 173.69470 | 620 | 240.55514 | 960 | 269.42172 |
| 290 | 176.97165 | 630 | 241.68500 | 970 | 270.06329 |
| 300 | 180.13094 | 640 | 242.79005 | 980 | 270.69624 |
| 310 | 183.17680 | 650 | 243.87139 | 990 | 271.32073 |
| 320 | 186.11338 | 660 | 244.93006 | 1000 | 271.93690 |
| 330 | 188.94476 | 670 | 245.96705 | - | - |
| 340 | 191.67494 | 680 | 246.98325 | - | - |

**Table S.12.** Calculated entropy function, S, of uranopilite. Temperature and entropy values are given in K and $J \cdot K^{-1} \cdot mol^{-1}$ units, respectively.

| T | S | T | S | T | S |
|---|---|---|---|---|---|
| 10 | 1.31059 | 350 | 238.96016 | 690 | 389.97832 |
| 20 | 5.23433 | 360 | 244.46993 | 700 | 393.55355 |
| 30 | 10.82512 | 370 | 249.89700 | 710 | 397.09172 |
| 40 | 17.50003 | 380 | 255.24348 | 720 | 400.59358 |
| 50 | 24.92055 | 390 | 260.51142 | 730 | 404.06018 |
| 60 | 32.84387 | 400 | 265.70271 | 740 | 407.49199 |
| 70 | 41.08322 | 410 | 270.81922 | 750 | 410.88985 |
| 80 | 49.49697 | 420 | 275.86304 | 760 | 414.25437 |
| 90 | 57.97786 | 430 | 280.83551 | 770 | 417.58631 |
| 100 | 66.45025 | 440 | 285.73875 | 780 | 420.88633 |
| 110 | 74.85873 | 450 | 290.57433 | 790 | 424.15490 |
| 120 | 83.16834 | 460 | 295.34369 | 800 | 427.39292 |
| 130 | 91.35614 | 470 | 300.04868 | 810 | 430.60073 |
| 140 | 99.40746 | 480 | 304.69062 | 820 | 433.77902 |
| 150 | 107.31581 | 490 | 309.27125 | 830 | 436.92839 |
| 160 | 115.07886 | 500 | 313.79184 | 840 | 440.04939 |
| 170 | 122.69623 | 510 | 318.25402 | 850 | 443.14246 |
| 180 | 130.17077 | 520 | 322.65885 | 860 | 446.20819 |
| 190 | 137.50556 | 530 | 327.00805 | 870 | 449.24706 |
| 200 | 144.70428 | 540 | 331.30278 | 880 | 452.25963 |
| 210 | 151.77142 | 550 | 335.54425 | 890 | 455.24633 |
| 220 | 158.71069 | 560 | 339.73389 | 900 | 458.20758 |
| 230 | 165.52688 | 570 | 343.87273 | 910 | 461.14386 |
| 240 | 172.22363 | 580 | 347.96200 | 920 | 464.05555 |
| 250 | 178.80468 | 590 | 352.00288 | 930 | 466.94326 |
| 260 | 185.27379 | 600 | 355.99643 | 940 | 469.80717 |
| 270 | 191.63416 | 610 | 359.94380 | 950 | 472.64786 |
| 280 | 197.88940 | 620 | 363.84592 | 960 | 475.46563 |
| 290 | 204.04207 | 630 | 367.70393 | 970 | 478.26095 |
| 300 | 210.09520 | 640 | 371.51877 | 980 | 481.03409 |
| 310 | 216.05166 | 650 | 375.29144 | 990 | 483.78548 |
| 320 | 221.91400 | 660 | 379.02288 | 1000 | 486.51546 |
| 330 | 227.68442 | 670 | 382.71386 | - | - |
| 340 | 233.36585 | 680 | 386.36545 | - | - |

**Table S.13.** Calculated enthalpy function, $\Delta H$ ($\Delta H=H_T-H_{298}$), of uranopilite. Temperature and enthalpy values are given in K and $J \cdot K^{-1} \cdot mol^{-1}$ units, respectively.

| T | $H_T-H_{298}$ | T | $H_T-H_{298}$ | T | $H_T-H_{298}$ |
|---|---|---|---|---|---|
| 10 | -3144.36773 | 350 | 27.72695 | 690 | 125.17629 |
| 20 | -1569.15170 | 360 | 32.38968 | 700 | 126.93763 |
| 30 | -1041.40548 | 370 | 36.86779 | 710 | 128.66298 |
| 40 | -775.19559 | 380 | 41.17354 | 720 | 130.35360 |
| 50 | -613.46754 | 390 | 45.31803 | 730 | 132.01068 |
| 60 | -503.95454 | 400 | 49.31136 | 740 | 133.63535 |
| 70 | -424.30740 | 410 | 53.16270 | 750 | 135.22869 |
| 80 | -363.38019 | 420 | 56.88044 | 760 | 136.79175 |
| 90 | -314.99435 | 430 | 60.47227 | 770 | 138.32549 |
| 100 | -275.44686 | 440 | 63.94526 | 780 | 139.83088 |
| 110 | -242.38017 | 450 | 67.30589 | 790 | 141.30880 |
| 120 | -214.21913 | 460 | 70.56018 | 800 | 142.76012 |
| 130 | -189.86903 | 470 | 73.71368 | 810 | 144.18566 |
| 140 | -168.54384 | 480 | 76.77152 | 820 | 145.58621 |
| 150 | -149.66353 | 490 | 79.73850 | 830 | 146.96253 |
| 160 | -132.79007 | 500 | 82.61905 | 840 | 148.31534 |
| 170 | -117.58611 | 510 | 85.41733 | 850 | 149.64532 |
| 180 | -103.78739 | 520 | 88.13721 | 860 | 150.95315 |
| 190 | -91.18389 | 530 | 90.78230 | 870 | 152.23946 |
| 200 | -79.60648 | 540 | 93.35601 | 880 | 153.50486 |
| 210 | -68.91746 | 550 | 95.86150 | 890 | 154.74994 |
| 220 | -59.00354 | 560 | 98.30177 | 900 | 155.97527 |
| 230 | -49.77067 | 570 | 100.67964 | 910 | 157.18137 |
| 240 | -41.14010 | 580 | 102.99774 | 920 | 158.36878 |
| 250 | -33.04539 | 590 | 105.25856 | 930 | 159.53799 |
| 260 | -25.43008 | 600 | 107.46446 | 940 | 160.68949 |
| 270 | -18.24587 | 610 | 109.61767 | 950 | 161.82373 |
| 280 | -11.45118 | 620 | 111.72028 | 960 | 162.94116 |
| 290 | -5.00999 | 630 | 113.77428 | 970 | 164.04221 |
| 300 | 1.10904 | 640 | 115.78155 | 980 | 165.12730 |
| 310 | 6.93336 | 650 | 117.74387 | 990 | 166.19681 |
| 320 | 12.48713 | 660 | 119.66294 | 1000 | 167.25114 |
| 330 | 17.79169 | 670 | 121.54037 | - | - |
| 340 | 22.86600 | 680 | 123.37767 | - | - |

**Table S.14.** Calculated free-energy function, function, $\Delta G$ ($\Delta G = G_T - H_{298}$), of uranopilite. Temperature and free-energy values are given in K and $J \cdot K^{-1} \cdot mol^{-1}$ units, respectively.

| T | $G_T$-$H_{298}$ | T | $G_T$-$H_{298}$ | T | $G_T$-$H_{298}$ |
|---|---|---|---|---|---|
| 10 | -3145.67848 | 350 | -211.23332 | 690 | -264.80205 |
| 20 | -1574.38608 | 360 | -212.08023 | 700 | -266.61587 |
| 30 | -1052.23141 | 370 | -213.02915 | 710 | -268.42868 |
| 40 | -792.69571 | 380 | -214.06988 | 720 | -270.24003 |
| 50 | -638.38848 | 390 | -215.19331 | 730 | -272.04948 |
| 60 | -536.79859 | 400 | -216.39131 | 740 | -273.85663 |
| 70 | -465.39078 | 410 | -217.65657 | 750 | -275.66113 |
| 80 | -412.87699 | 420 | -218.98254 | 760 | -277.46262 |
| 90 | -372.97237 | 430 | -220.36330 | 770 | -279.26081 |
| 100 | -341.89686 | 440 | -221.79352 | 780 | -281.05540 |
| 110 | -317.23910 | 450 | -223.26837 | 790 | -282.84613 |
| 120 | -297.38777 | 460 | -224.78350 | 800 | -284.63276 |
| 130 | -281.22512 | 470 | -226.33495 | 810 | -286.41506 |
| 140 | -267.95144 | 480 | -227.91911 | 820 | -288.19283 |
| 150 | -256.97960 | 490 | -229.53272 | 830 | -289.96589 |
| 160 | -247.86898 | 500 | -231.17280 | 840 | -291.73404 |
| 170 | -240.28255 | 510 | -232.83662 | 850 | -293.49715 |
| 180 | -233.95827 | 520 | -234.52171 | 860 | -295.25507 |
| 190 | -228.68940 | 530 | -236.22579 | 870 | -297.00765 |
| 200 | -224.31073 | 540 | -237.94679 | 880 | -298.75478 |
| 210 | -220.68872 | 550 | -239.68281 | 890 | -300.49636 |
| 220 | -217.71430 | 560 | -241.43211 | 900 | -302.23228 |
| 230 | -215.29754 | 570 | -243.19308 | 910 | -303.96245 |
| 240 | -213.36369 | 580 | -244.96426 | 920 | -305.68679 |
| 250 | -211.85009 | 590 | -246.74430 | 930 | -307.40523 |
| 260 | -210.70387 | 600 | -248.53195 | 940 | -309.11769 |
| 270 | -209.88013 | 610 | -250.32608 | 950 | -310.82413 |
| 280 | -209.34050 | 620 | -252.12564 | 960 | -312.52449 |
| 290 | -209.05200 | 630 | -253.92965 | 970 | -314.21873 |
| 300 | -208.98616 | 640 | -255.73723 | 980 | -315.90679 |
| 310 | -209.11826 | 650 | -257.54756 | 990 | -317.58866 |
| 320 | -209.42677 | 660 | -259.35988 | 1000 | -319.26430 |
| 330 | -209.89283 | 670 | -261.17349 | - | - |
| 340 | -210.49988 | 680 | -262.98774 | - | - |

**Table S.15.** Calculated enthalpies ($\Delta_r H$) and free-energies ($\Delta_r G$) of reaction and associated reaction constants (Log K) of reactions (A)-(F). The values of $\Delta_r H$ and $\Delta_r G$ are in units of $kJ \cdot mol^{-1}$.

| T(K) | $\Delta_r H$ | $\Delta_r G$ | $Log\ K$ | $\Delta_r H$ | $\Delta_r G$ | $Log\ K$ |
|---|---|---|---|---|---|---|
| | **Reaction (A)** | | | **Reaction (B)** | | |
| 298.15 | -64.11 | -26.86 | 4.70 | -39.22 | -13.22 | 2.32 |
| 300 | -63.89 | -26.18 | 4.56 | -39.06 | -12.75 | 2.22 |
| 320 | -61.85 | -19.20 | 3.13 | -37.51 | -7.91 | 1.29 |
| 340 | -60.34 | -12.68 | 1.95 | -36.37 | -3.44 | 0.53 |
| 360 | -59.02 | -6.29 | 0.91 | -35.39 | 0.93 | -0.13 |
| 380 | -58.68 | -0.79 | 0.11 | -35.07 | 4.69 | -0.64 |
| 400 | -58.43 | 4.69 | -0.61 | -34.83 | 8.42 | -1.10 |
| 420 | -58.52 | 9.91 | -1.23 | -34.82 | 11.97 | -1.49 |
| 440 | -58.93 | 14.91 | -1.77 | -35.04 | 15.36 | -1.82 |
| 460 | -59.66 | 19.69 | -2.24 | -35.48 | 18.61 | -2.11 |
| 480 | -60.69 | 24.30 | -2.64 | -36.13 | 21.72 | -2.36 |
| 500 | -62.03 | 28.74 | -3.00 | -37.00 | 24.72 | -2.58 |
| **T(K)** | **Reaction (C)** | | | **Reaction (D)** | | |
| 298.15 | 22.68 | 11.15 | -1.95 | -6.46 | 23.14 | -4.09 |
| 300 | 22.74 | 11.35 | -1.98 | -6.43 | 23.51 | -4.09 |
| 320 | 23.12 | 13.42 | -2.19 | -6.25 | 27.36 | -4.47 |
| 340 | 23.18 | 15.26 | -2.34 | -6.26 | 31.05 | -4.77 |
| 360 | 23.25 | 17.18 | -2.49 | -6.26 | 34.81 | -5.05 |
| 380 | 22.51 | 18.37 | -2.53 | -6.77 | 38.11 | -5.24 |
| 400 | 21.81 | 19.71 | -2.57 | -7.24 | 41.50 | -5.42 |
| 420 | 20.90 | 20.93 | -2.60 | -7.83 | 44.82 | -5.57 |
| 440 | 19.77 | 22.04 | -2.62 | -8.55 | 48.08 | -5.71 |
| 460 | 18.42 | 23.05 | -2.62 | -9.39 | 51.28 | -5.82 |
| 480 | 16.84 | 23.97 | -2.61 | -10.36 | 54.43 | -5.92 |
| 500 | 15.03 | 24.83 | -2.59 | -11.47 | 57.53 | -6.01 |
| **T(K)** | **Reaction (E)** | | | **Reaction (F)** | | |
| 298.15 | 49.61 | 42.15 | -7.38 | -27.83 | -14.46 | 2.53 |
| 300 | 49.52 | 41.97 | -7.31 | -27.76 | -14.21 | 2.47 |
| 320 | 48.73 | 40.21 | -6.56 | -27.08 | -11.56 | 1.89 |
| 340 | 48.10 | 38.60 | -5.93 | -26.52 | -9.02 | 1.39 |
| 360 | 47.56 | 37.08 | -5.38 | -26.10 | -6.60 | 0.96 |
| 380 | 47.20 | 35.73 | -4.91 | -25.81 | -4.30 | 0.59 |
| 400 | 46.91 | 34.44 | -4.50 | -25.66 | -2.13 | 0.28 |
| 420 | 46.72 | 33.25 | -4.13 | -25.62 | -0.08 | 0.01 |
| 440 | 46.61 | 32.13 | -3.81 | -25.70 | 1.88 | -0.22 |
| 460 | 46.60 | 31.09 | -3.53 | -25.87 | 3.74 | -0.43 |
| 480 | 46.67 | 30.12 | -3.28 | -26.13 | 5.53 | -0.60 |
| 500 | 46.82 | 29.21 | -3.05 | -26.50 | 7.26 | -0.76 |

**References**


[1] S. J. Clark, M. D. Segall. C. J. Pickard, P. J. Hasnip, M. I. J. Probert, K. Refson, M. C. Payne, *Z. Kristallogr*., 2020, **220**, 567–570.

[2] MaterialsStudio http://3dsbiovia.com/products/collaborative-science/biovia-materials-studio/, accessed 15 April, 2020.

[3] M. C. Payne, M. P. Teter, D. C. Ailan, A. Arias, J. D. Joannopoulos, *Rev. Mod. Phys*., 1992, **64**, 1045–1097.

[4] J. P. Perdew, K. Burke, M. Ernzerhof, *Phys. Rev. Lett*., 1996, **77**, 3865–3868.

[5] S. Grimme, *J. Comput. Chem*., 2006, **27**, 1787–1799.

[6] N. Troullier, J. L. Martins, *Phys. Rev. B*, 1991, **43**, 1993–2006.

[7] L. J. Bonales, F. Colmenero, J. Cobos, V. Timón, *Phys. Chem. Chem. Phys*., 2006, **18**, 16575–16584.

[8] F. Colmenero, *Characterization of Secondary Phases of Spent Nuclear Fuel under Final Geological Disposal Conditions: Experimental and Theoretical Studies*, PhD Thesis, Universidad Autónoma de Madrid, Madrid, 2017; https://doi.org/ 10.13140/RG.2.2.10526.43843.

[9] F. Colmenero, L. J. Bonales, J. Cobos, V. Timón, *J. Phys. Chem. C,* 2017, **121**, 14507−14516.

[10] F. Colmenero, A. M. Fernández, J. Cobos, V. Timón, *J. Phys. Chem. C*, 2018, **122**, 5254−5267.

[11] F. Colmenero. A. M. Fernández, J. Cobos, V. Timón, *J. Phys. Chem. C*, 2018, **122**, 5268−5279.

[12] F. Colmenero, J. Cobos, V. Timón, *Inorg. Chem*., 2018, **57**, 4470−4481.

[13] F. Colmenero, in *Minerals*, ed. K. S. Essa, InTechOpen, London, 2018, ch. 4; pp. 65−94.

[14] F. Colmenero, in *Density Functional Theory*, ed. D. Glossman-Mitnik, InTechOpen, London, 2018, ch. 5; pp. 91−122.

[15] F. Colmenero, A. M. Fernández, V. Timón, J. Cobos, *RSC Adv*., 2018, **8**, 24599−24616.

[16] F. Colmenero, J. Plášil, J. Cobos, J. Sejkora, V. Timón, J. Čejka, L. J. Bonales, *RSC Adv*., 2019, **9**, 15323–15334.

[17] F. Colmenero, J. Plášil, J. Cobos, J. Sejkora, V. Timón, J. Čejka, A. M. Fernández, V. Petříček, *RSC Adv*., 2019, **9**, 40708–40726.

[18] F. Colmenero, J. Plášil, J. Sejkora, *Dalton Trans*., 2019, **48**, 16722–16736.

[19] B. G. Pfrommer, M. Cote, S. G. Louie, M. L. Cohen, *J. Comput. Phys*., 1997, **131**, 233–240.

[20] H. J. Monkhorst, J. D. Pack, *Phys. Rev. B*, 1976, **13**, 5188–5192.

[21] R. T. Downs, K. L. Bartelmehs, G. V. Gibbs, M. B. Boisen, *Am. Mineral*., 1993, **78**. 1104–1107.

[22] M. Cococcioni, in *Correlated Electrons: From Models to Materials Modeling and Simulation*, Vol. 2, ed. Pavarini *et al*., Forschungszentrum Jülich, Berlin, 2012, ch. 4.

[23] S. L. Dudarev, D. Nguyen-Manh, A. P. Sutton, *Phil. Mag. B*, 1997, **75**, 613–628.

[24] J. P. Crocombette, F. Jollet, L. T. Nga, T. Petit, *Phys. Rev. B*, 2001, **64**, 104107.

[25] P. F. Weck, E. Kim, C. F. Jové-Colón, D. C. Sassani, *Dalton Trans*., 2013, **42**, 4570–4578.

[26] D. A. Andersson, G. Baldinozzi, L. Desgranges, D. R. Conradson, S. R. Conradson*, Inorg. Chem*., 2013, **52**, 2769−2778.

[27] G. Beridze, P. M. Kowalski, *J. Phys. Chem. A*, 2014, **118**, 11797−11810.

[28] P. F. Weck, E. Kim, *Dalton Trans*., 2004, **43**, 17191–17199.

[29] P. F. Weck, E. Kim, E. C. Buck, *RSC Adv.*, 2015, **5**, 79090 −79097.

[30] P. F. Weck, E. Kim, J*. Phys. Chem. C*, 2016, **120**, 16553 −16560.

[31] T. M. Alam, Z. Liao, M. Nyman, J. Yates, *J. Phys. Chem. C*, 2016, **120**, 10675−10685.

[32] N. Kalashnyk, D. L. Perry, F. Massuyeau, E. Faulques, *J. Phys. Chem. C*, 2018, **122**, 7410−7420.

[33] S. Ostanin, P. Zeller, *J. Phys.: Condens. Matter*., 2007, **19**, 246108.

[34] S. Ostanin, P. Zeller, *Phys. Rev. B*, 2007, **75**, 073101.

[35] J. F. Nye, *Physical Properties of Crystals*, Clarendon, Oxford, 1976.
[36] R. Yu, J. Zhu, H. Q. Ye, *Comput. Phys. Commun*., 2010, **181**, 671−675.
[37] F. Birch, *Phys. Rev*., 1947, **71**, 809−824.
[38] R. J. Angel, *Rev. Mineral. Geochem*., 2000, **41**, 35−60.
[39] EOSFIT 5.2 software, http://programming.ccp14.ac.uk/ccp/web-mirrors/ross-angel/crystal/software.html, accessed 15 April, 2020.
[40] A. S. H. Marmier, Z. A. D. Lethbridge, R. I. Walton, C. W. Smith, S. C. Parker, K. E. Evans, *Comput. Phys. Commun*., 2010, **81**, 2102−2115.
[41] S. Baroni, S. de Gironcoli, A. Dal Corso, P. Giannozzi, *Rev. Mod. Phys*., 2001, **73**, 515–562.
[42] K. Refson, P. R. Tulip, S. J. Clark, *Phys. Rev. B*, 2006, **73**, 155114.
[43] W. J. Hehre, L. Radom, P. V. R. Schleyer, J. A. People, *Ab Initio Molecular Orbital Theory*, Wiley, New York, 1986.
[44] C. Lee, X. Gonze, *Phys. Rev. B*, 1995, **51**, 8610–8613.
[45] M. W. Chase, C. A. Davies, J. R. Downey, D. J. Frurip, R. A. McDonald, A. N. Syverud, *J. Phys. Chem. Ref. Data*, 1985, **14** [Suppl 1], 1–1856.
[46] I. Barin, *Thermochemical Data of Pure Substances. Third edition*, VCH, Weinheim, 1995.
[47] R. L. Frost, J. Čejka, M. L. Weier, W. Martens, G. A. Ayoko, *J. Raman Spectrosc*., 2007, **38**, 398–409.
[48] P. C. Burns, *Can. Mineral*., 2001, **39**, 1139–1146.